

# A twisted tale of the transverse-mass tail

---

**Triparno Bandyopadhyay,<sup>a</sup> Ankita Budhraja,<sup>b</sup> Samadrita Mukherjee,<sup>b</sup> Tuhin S. Roy<sup>b</sup>**

<sup>a</sup>*Department of Physics,  
Indian Institute of Technology Kanpur,  
Kanpur 208016, India.*

<sup>b</sup>*Department of Theoretical Physics,  
Tata Institute of Fundamental Research,  
1, Homi Bhabha Road, Colaba,  
Mumbai 400005, India.*

*E-mail:* [triparno@theory.tifr.res.in](mailto:triparno@theory.tifr.res.in), [ankita.budhraja@tifr.res.in](mailto:ankita.budhraja@tifr.res.in),  
[samadrita.mukherjee@tifr.res.in](mailto:samadrita.mukherjee@tifr.res.in), [tuhin@theory.tifr.res.in](mailto:tuhin@theory.tifr.res.in)

**ABSTRACT:** We propose a tantalizing possibility that misinterpretation of the reconstructed missing momentum may have yielded the observed discrepancies among measurements of the  $W$ -mass in different collider experiments. We introduce a proof-of-principle scenario characterized by a new physics particle, which can be produced associated with the  $W$ -boson in hadron collisions and contributes to the net missing momentum observed in a detector. We show that these exotic events pass the selection criteria imposed by various collaborations at reasonably high rates. Consequently, in the presence of even a handful of these events, a fit based on the ansatz that the missing momentum is primarily due to neutrinos (as it happens in the Standard Model), yields a  $W$ -boson mass that differs from its true value. Moreover, the best fit mass depends on the nature of the collider and the center-of-mass energy of collisions. We construct a barebones model that demonstrates this possibility quantitatively while satisfying current constraints. Interestingly, we find that the nature of the new physics particle and its interactions appear as a variation of the physics of Axion-like particles after a field redefinition.

It has been over a decade since the discovery of the Higgs boson at the Large Hadron Collider (LHC). Unfortunately, the large set of searches designed to look for traces of physics beyond the Standard Model (BSM) of particle physics has only returned empty-handed without any definitive signature of new physics (NP). More importantly, all searches that we have designed in order to discover the “well-motivated” models, which are constructed to address/solve a host of issues ranging from naturalness to dark matter, have only yielded exclusion plots (see, e.g., [1–13]). On the other hand, there have been exciting but scattered *hints* of NP emerging from the intensity frontier and from cosmological measurements (see, e.g., [14–17]). Not surprisingly, considerable efforts have gone into interpreting these *anomalies* in terms of BSM physics.

The recent (and the most precise) measurement of the  $W$ -boson mass ( $M_W$ ) by the CDF collaboration of Tevatron [18] has given rise to much excitement. After analyzing  $8.8 \text{ fb}^{-1}$  of data, the collaboration finds the  $M_W$  measurement to be *incompatible* with all previous direct and indirect measurements in a statistically significant way:

$$\begin{aligned} M_W &= 80.4335 \pm 0.0094 \text{ GeV} & : & \text{CDF [18]}, \\ M_W &= 80.370 \pm 0.019 \text{ GeV} & : & \text{ATLAS [19]}, \\ M_W &= 80.354 \pm 0.023 \text{ GeV} & : & \text{LHCb [20]}, \\ M_W &= 80.3545 \pm 0.0057 \text{ GeV} & : & \text{Precision Electroweak [21]}. \end{aligned} \tag{1}$$

These large discrepancies (along with various LEP results [22–25]), primarily stemming from the impressive control of systematics in the CDF measurement, are unexpected. At this juncture, one can attribute the anomaly to underestimated/unaccounted-for systematics, and simply wait for future measurements from the LHC before speculating over possible BSM implications.

In this work, we take a contrasting viewpoint and attempt to find an interpretation where these measurements (both direct and indirect) can be made compatible with each other. Note that, to date, there have been multiple proposals exploring a plethora of BSM solutions (see, e.g., [26–50]) along with various proposed corrections to electroweak (EW) precision observables (see [51–60] and references therein), to address the discrepancy. The underlying theme for all these attempts is to introduce NP which modifies precision EW observables such that the precision fit of the  $M_W$  becomes compatible with the CDF measurement, therefore, ignores all other direct measurements.

The discrepancy between the CDF measurement of  $M_W$  and that predicted by EW precision fits may in itself be taken to be a hint for BSM physics. However, when compared with the other *experimental measurements* by ATLAS, LHCb, and LEP, which are consistent with each other and with the EW fit at  $1\sigma$ , the implications of the CDF result become much more nuanced. In this work, we attempt to address the question of whether one can reconcile the CDF value of  $M_W$  not just with the EW precision fit but also with measurements from other colliders. In particular, we ask whether an NP interpretation exists where  $M_W$  remains the same as the precision EW fit, but its measurements at different colliders yield differing values.

Remarkably, we do find such a scenario. The all-important observation which allows us to reconcile these different measurements is that precise  $M_W$  measurements rely on leptonic decays of  $W$  which give rise to neutrinos in the final state. Since the exact reconstruction of the  $W$  four-vector is not possible, experimental collaborations use various kinematic variables sensitive to the  $W$ -boson mass, the most important of which is the transverse mass,  $M_T$ . It is defined using only the transverse components of the lepton momentum ( $p^\ell$ ) and the missing transverse momentum (namely,  $\vec{p}_T^{\text{miss}}$ ).

$$M_T^2 \equiv 2 \left( p_T^\ell p_T^{\text{miss}} - \vec{p}_T^\ell \cdot \vec{p}_T^{\text{miss}} \right), \quad \text{where} \quad (2)$$

$$p_T^\ell = \sqrt{\vec{p}_T^\ell \cdot \vec{p}_T^\ell} \quad \text{and} \quad p_T^{\text{miss}} = \sqrt{\vec{p}_T^{\text{miss}} \cdot \vec{p}_T^{\text{miss}}}.$$

Note that, if the missing momentum is entirely due to the missing neutrino from  $W$  decay, the transverse mass shows a kinetic endpoint at  $M_T \leq M_W$ . Even though smearing, energy mismeasurements, and hadronic activities (especially in proton colliders) in the event soften the kinematic edge, a precise extraction of  $M_W$  is possible after taking various systematics into consideration, with the underlying assumption that the missing momentum is mostly due to the neutrino from  $W$ -decay. We find that breaking this assumption slightly gives us the desired result. If NP gives rise to events where a  $W$  is produced along with a BSM invisible state, say  $\Phi$ , the missing momentum observed in these events becomes larger than the neutrino transverse momenta. Using the definition of Equation (2), it is a straightforward exercise to show that

$$M_T \Big|_{\vec{p}_T^{\text{miss}} = \vec{p}_T^\nu + \vec{p}_T^\Phi} \geq M_T \Big|_{\vec{p}_T^{\text{miss}} = \vec{p}_T^\nu}. \quad (3)$$

Therefore, if these events pass event selection criteria as designed by the experiments, one expects more events at the tail of the  $M_T$  distribution. We intuit that if this entire set of events, i.e., Standard Model (SM) single  $W$ -events + SM background events + NP events, is fitted with the SM-only hypothesis to find the  $W$ -mass, one inadvertently obtains the best fit to be slightly larger than the true  $M_W$ .

The working principle in our framework is therefore rather simple: (*i.*) we need a light NP particle,  $\Phi$ , which decays mostly to the dark sector (or sufficiently long-lived), so that it gives rise to missing momentum in the detector; and (*ii.*) we need an irrelevant operator that allows for the production  $p + \bar{p}(p) \rightarrow W + \Phi$ . In this paper, we show that such a naive set-up accommodates the CDF measurement of  $M_W$ , with the precision electroweak measurement on one hand, and with results from LEP, ATLAS, and from LHCb on the other. We take  $\Phi$  to be a real scalar (SM gauge singlet) and invoke the following operator

$$\frac{\kappa}{\Lambda} g_w W_\mu^+ \Phi \bar{u}_L \gamma^\mu d_L + \text{h.c.}, \quad (4)$$

where  $\kappa$  is a dimensionless complex coupling constant,  $\Lambda$  is the scale of the irrelevant operator, and  $g_w$  is the weak coupling constant. Apart from this, we also assume that  $\Phi$  decays mostly to the dark sector. Even though Equation (4) implies a non-zero width of  $\Phi$  to SM (if allowed by kinematics), this width would be phase-space and  $m_\Phi^2/\Lambda_{\text{eff}}^2$  suppressed, where  $\Lambda_{\text{eff}} = \Lambda/|\kappa|$  is the *effective* scale of the operator. Consequently, the fractional width

of  $\Phi$  to SM can be made negligible by assuming marginal coupling of  $\Phi$  to the dark sector. The physics of  $M_W$  measurement is, however, independent of the details of such couplings and, therefore, we do not present any explicit model of dark- $\Phi$  interactions.

As we show next, this minimal and naive set-up is sufficient for the purpose of resolving the discrepancies observed around the  $W$ -mass measurement. After determining  $\Lambda_{\text{eff}}$ , we discuss observables that may constrain the existence of  $\Phi$  and its interaction in Equation (4). Later, we dig deep into understanding the origin of the crucial operator in Equation (4), which compels us to consider questions regarding aspects of EW symmetry. We provide several scenarios which allow us to address these questions. It is outside the scope of this work to give a complete classification of all possible models of ultraviolet (UV) physics that may lead to our *effective* theory of  $W$ -mass anomaly and to study phenomenological consequences of all these different classes. We leave these for future endeavors.

The central purpose of the next part of the paper is to support our claim through quantitative statements, for which we use simulations. However, before we begin with the details, here we take a pause to discuss our general approach. We divide our studies into three main segments. We begin with studies relevant to the  $M_W$  measurements at the CDF, at the ATLAS, and at the LHCb (as given in Equation (1)) in order to map the strength of the operator in Equation (4) to these experiments. In the second part, we discuss other measurements/searches which directly get impacted because of this same operator and derive present constraints. Once we obtain the allowed space for NP consistent with all the observables discussed, we make predictions for future  $M_W$  measurements at the LHC (at 13 TeV and with a high luminosity).

From our simulations, it is clear that—by construction—a sizable fraction of NP events pass the set of cuts, which are designed to select a pure sample of SM  $W$  events in any of these experiments. The number of such NP events depends not just on the colliding particles but also on the center-of-mass energy of collisions and the cuts themselves. Therefore, the shift in the fitted  $M_W$  from its true value should be critically dependent on the specificity of the analysis. The task of calculating the effect of Equation (4) in the determination of  $M_W$ , therefore, requires a careful understanding and reproduction of the analyses performed by each of these collaborations. This task is rather difficult (especially in the context of Tevatron analyses) since efficient and vetted fast-simulators for CDF or D0 are not available readily. This implies that it is simply not feasible to fit the “observed data” to determine the Wilson coefficient in Equation (4). In this work, we, therefore, take an alternate approach. We use the range of  $M_W$  (as reported by the corresponding experimental collaborations) that best represents the observed-data, to determine the strength of the operator in Equation (4).

Even though the details of the exact procedures we employ for different measurements in Equation (1) are far removed from each other, here we summarize the steps that characterize all these studies.

- In this work, we choose the true mass of the  $W$ -boson (denoted by  $\widehat{M}_W$  from now on) to be the one determined using precision electroweak observables.

$$\widehat{M}_W = 80.3545 \pm 0.0057 \text{ GeV} . \quad (5)$$

	Tevatron $p + \bar{p}$ @ 1.96 TeV	ATLAS $p + p$ @ 7 TeV	LHCb $p + p$ @ 13 TeV
Generator level cuts	$-1.2 \leq \eta^\ell \leq 1.2$ $p_T^\ell \geq 10 \text{ GeV}$ $p_T^j \geq 20 \text{ GeV}$	$-2.7 \leq \eta^\ell \leq 2.7$ $p_T^\ell \geq 10 \text{ GeV}$ $p_T^j \geq 20 \text{ GeV}$	$1.8 \leq \eta^\ell \leq 5.2$ $p_T^\ell \geq 10 \text{ GeV}$ $p_T^j \geq 20 \text{ GeV}$
$\mathcal{X}$	$\{M_T, p_T^\ell, p_T^{\text{miss}}\}$	$\{M_T, p_T^\ell, p_T^{\text{miss}}\}$	$\{p_T^\ell\}$
Selection cuts	$-1.0 < \eta^\ell < 1.0$ $30 < p_T^\ell (\text{GeV}) < 55$ $30 < p_T^{\text{miss}} (\text{GeV}) < 55$ $60 < M_T (\text{GeV}) < 100$ $u_T < 15 \text{ GeV}$	$-2.5 < \eta^\ell < 2.5$ $p_T^\ell > 30 \text{ GeV}$ $p_T^{\text{miss}} > 30 \text{ GeV}$ $M_T > 60 \text{ GeV}$ $u_T < 30 \text{ GeV}$	$2.2 < \eta^\ell < 4.4$ $28 < p_T^\ell (\text{GeV}) < 52$
Fitting range	$32 \leq p_T^\ell (\text{GeV}) \leq 48$ $32 \leq p_T^{\text{miss}} (\text{GeV}) \leq 48$ $65 \leq M_T (\text{GeV}) \leq 90$	$32 \leq p_T^\ell (\text{GeV}) \leq 45$ $32 \leq p_T^{\text{miss}} (\text{GeV}) \leq 45$ $66 \leq M_T (\text{GeV}) \leq 99$	$28 < p_T^\ell (\text{GeV}) < 52$

**Table 1.** Cuts and selection criteria for simulating events  $W(\ell\nu) + \text{jets}$  for CDF, for ATLAS@7 TeV and for LHCb@13 TeV.

- Using  $M_W = \widehat{M}_W$ , we generate a large sample of matched  $W(\ell\nu) + \text{jets}$  events at the parton level for which we utilize **MadGraph-v3.4.1** [61]. The inputs to the matrix element generators are a set of parton level cuts, which we list under Table 1, a factorization/renormalization scale, and a parton distribution function (PDF) set. For factorization/renormalization scales, we use the default **MadGraph** values, whereas for PDF we use NNPDF23\_NLO [62, 63]. Subsequently, all parton level events are passed through **Pythia-v8.306** [64] for showering and hadronization. In order to avoid double counting, we employ the MLM scheme [65] and use  $\text{xqcut} = 30 \text{ GeV}$ . We use **Delphes-v3.5.0** [66] to provide a realistic detector environment whenever we can. For ATLAS, we use the default card as provided in **Delphes**. We will mention additional steps/details specific to individual measurements later.
- We impose selection cuts as tabulated in Table 1. Note that we closely follow the cuts as given in the respective experimental reports [18–20]. These sets of cuts consist of variables already discussed previously in Equation (2), except for pseudo-rapidity for the lepton (namely,  $\eta^\ell$ ) and the transverse hadronic recoil variable  $u_T$ . The working definition of  $u_T$  employed in this work is collider specific and so we describe it later.
- We analyze the final sample of selected events and calculate observables. For the rest

of this work, we denote the set of observables needed for estimating  $M_W$  to be  $\mathcal{X}$ . For example, in case of CDF  $\mathcal{X}$  consists of  $\{M_T, p_T^\ell, p_T^{\text{miss}}\}$  defined in Equation (2). This list is also summarized in Table 1. The outcomes of this step are histograms corresponding to the variables in  $\mathcal{X}$ —i.e., for every observable  $x \in \mathcal{X}$  we obtain a Histogram  $X$  which represents  $\mathcal{L} \times d\sigma/dX$ ,  $\mathcal{L}$  being the integrated luminosity.

- We *repeat* all the steps above after setting  $M_W = \widehat{M}_W + \Delta$ , where  $\Delta$  represents the shift in the mass parameter. We denote histograms of the variable  $x$  for a given  $\Delta$  by  $X(\Delta)$ . In this notation, therefore, histograms for  $M_W = \widehat{M}_W$  are simply  $X(0)$ .
- We also require simulated event samples for NP. We implement the operator of Equation (4) into **MadGraph** and repeat the above procedure to generate corresponding histograms. For NP, we denote these histograms by  $X^{\text{NP}}(\Lambda_{\text{eff}})$ , because of its obvious dependence on  $\Lambda_{\text{eff}}$ .
- Finally, for each values of  $\Delta$  we find the preferred value of  $\Lambda_{\text{eff}}$  by minimizing the function  $\mathcal{D}^2$  defined via

$$\mathcal{D}^2 = \sum_{x \in \mathcal{X}} \sum_b \left( \frac{X_b(\Delta) - X_b(0) - X_b^{\text{NP}}(\Lambda_{\text{eff}})}{\sigma_b^X} \right)^2. \quad (6)$$

In the above,  $X_b$  represents the number of events in the bin  $b$  of the histogram  $X$ , and  $(\sigma_b^X)^2$  is the variance of the same bin. The sum runs over all bins in the fitting range. We specify the fitting range for the three measurements in Table 1.

Before we summarize the results of our study, we need to mention analysis-specific details. Even though we mention  $W \rightarrow \ell\nu$  states in Table 1, we work with  $W \rightarrow e\nu_e$  for Tevatron and ATLAS, whereas we use  $W \rightarrow \mu\nu_\mu$  for LHCb. As mentioned before, we employ semi-realistic detector environments as implemented in **Delphes** for our ATLAS study. For Tevatron and for LHCb, we simply proceed directly to the analysis stage skipping the detector-simulation step. Since muons at the LHCb are well reconstructed with high efficiency and the muon  $p_T$  is the only observable, we expect our results for LHCb to be realistic. For Tevatron, however, the results are sensitive to details. In an Appendix, we show comparisons of confidence bands that correspond to different levels of detail (but using the same set of cuts in Table 1). In particular, we show the difference of analyzing directly using the output of **Pythia**, after taking into account QED corrections given by **ResBos-v2.0** [67] utilizing Reference [68], and finally after taking into account smearing as given in Reference [68]. Also, in the Appendix, we discuss the differences in using only the  $M_T$  variable for minimization in contrast to combining all the three variables  $\{M_T, p_T, p_T^{\text{miss}}\}$ . Given these issues, we choose to use histograms after **ResBos2** for all three variables but with a broad range of systematics (0–5%) that mostly captures the uncertainty with our Tevatron-specific analyses.

Finally, note that both the CDF and the ATLAS collaboration use the variable  $u_T$  which is a measure of the hadronic recoil. An upper cut on the hadronic recoil preferably selects  $W$  with small  $p_T$ . For Tevatron, we use the sum of all momenta for all final state

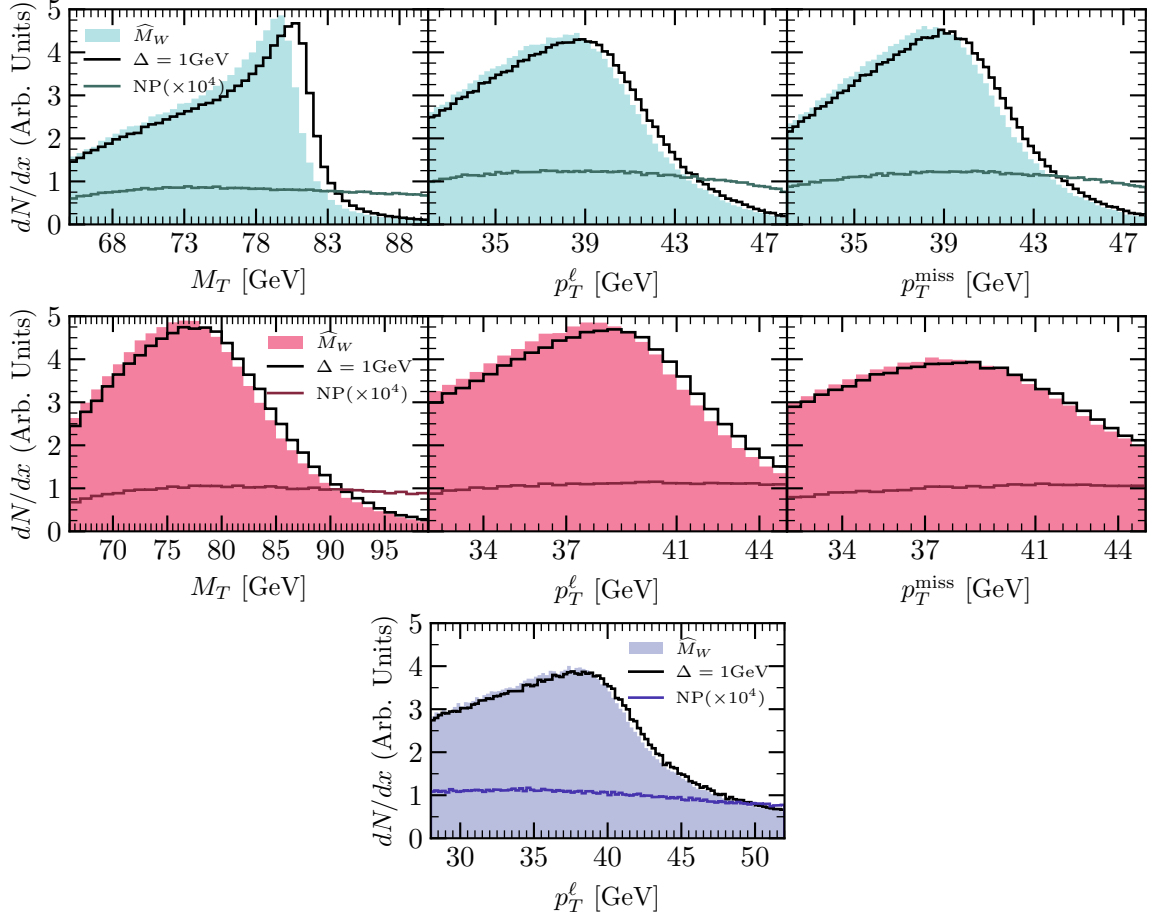


**Figure 1.** Distributions of different kinematic variables corresponding to CDF (top), ATLAS (middle) and LHCb (bottom). In each row, the left, center, and the right plot shows the histogram corresponding to  $M_T$ ,  $p_T^\ell$ , and  $p_T^{\text{miss}}$  respectively. In each panel, the different histograms correspond to SM with  $\Delta = 0$  (shaded),  $\Delta = 1$  GeV (black line) (large  $\Delta$  chosen for demonstration), and the NP process with  $\Lambda_{\text{eff}} = 1$  TeV (colored line). For legibility, we scale the NP numbers by  $10^4$ .

hadrons and photons within  $|\eta| \leq 3.6$  to calculate the recoil, whereas for ATLAS we use the sum of all jets and photons within  $|\eta| \leq 4.9$ .

We plot all the histograms that play a role in determining  $M_W$  in Figure 1. In each of these plots we show these distributions corresponding to  $M_W = \widehat{M}_W$  (shaded) and for  $M_W = \widehat{M}_W + \Delta$  (black lines), where for numerical demonstration we have taken  $\Delta = 1$  GeV. In each of these variables, there is a characteristic scale (related to the mass of  $W$ -boson), beyond which the distribution falls. A larger  $M_W$  increases the characteristic scale, which results in a rightward shift of the edge of  $M_T$  and slightly harder  $p_T^\ell$  and  $p_T^{\text{miss}}$ . On the other hand, the same plots for the NP events (evaluated here for  $\Lambda_{\text{eff}} = 1$  TeV, shown by colored lines, and scaled by  $10^4$  for legibility) have comparatively flatter distributions in the range of the plot. Consequently, these add “relatively” more events in the bins where SM distribution falls rapidly, shifting the histograms slightly towards larger values of the kinematic variables. Therefore, as argued at the beginning of this work, the distribution



for  $M_W = \widehat{M}_W$  when combined with a suitably weighted NP distribution may mimic the shape corresponding to a higher  $M_W$ .

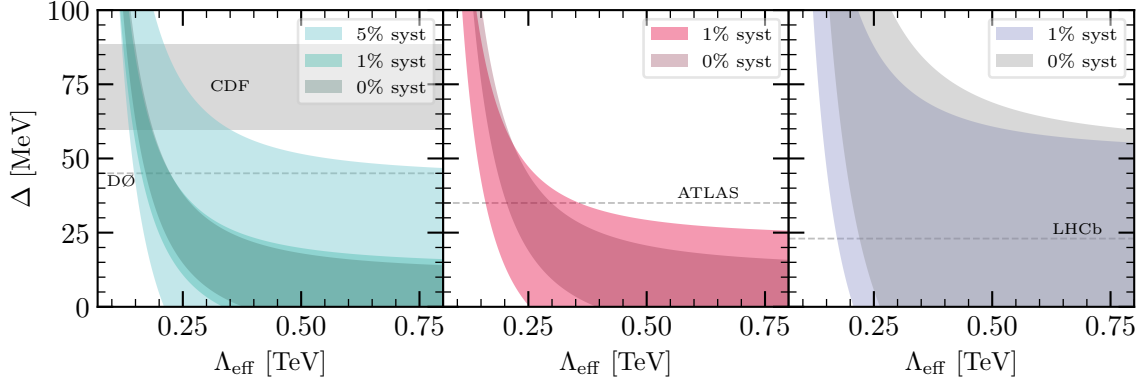


**Figure 2.** *Left:* 68% CL bands corresponding to 0%, 1%, and 5% systematic uncertainties for the CDF experiment overlaid on the CDF (+ResBos2 [68]) and D0 measurements of  $M_W$  at  $1\sigma$ . *Centre:* 68% bands corresponding to ATLAS, overlaid on the ATLAS  $M_W$  measurement at  $1\sigma$ . *Right:* 68% band for LHCb overlaid on the LHCb  $M_W$  measurement using  $p_T^\ell$  only.

Following the recipe described above, we can determine the confidence belts in  $\Lambda_{\text{eff}}$  for each value of  $\Delta$ . Note, however, that the location of the minimum of  $\mathcal{D}^2$  in Equation (6), as well as the width of the confidence belt depends on the assigned variance in each bin of the histogram. The statistical component of the variance is rather straightforward. Using the notation established above, we take  $(\sigma_b^X)^2|_{\text{stat}} = X_b(\Delta)$ . As explained before, we also need to add a systematics component to the variance, which reflects the uncertainties due to scale, generator, detector elements, etc. To take this into account, we perform our analysis by varying the systematics between 0% and 5%.

We give the result of the minimization procedure in the three plots of Figure 2 corresponding to CDF (left), ATLAS@7 TeV (center), and LHCb (right). As mentioned before, we are more prone to systematics in the context of Tevatron analyses, because of which we show the 68% confidence level (CL) contours for 5% systematics, in addition to the 0% and 1% ones. Note that, while extracting the bands for the CDF analysis, we convoluted the histograms generated after *Pythia* simulations by the bin-by-bin  $N^3\text{LL} + \text{NNLO}$  factors as given by the *ResBos2* package and quoted in Reference [68]. We indicate, using dotted lines, the upper limits of the  $M_W$  measurements reported by D0, ATLAS, and the LHCb collaborations, and with the shaded region we show the  $1\sigma$  limits corresponding to CDF. Note that, for the CDF  $1\sigma$  range, we have allowed for the possible 10 MeV downward shift, as reported in Reference [68].

Our first observation is that  $\Lambda_{\text{eff}} \rightarrow \infty$ , which corresponds to  $\kappa \rightarrow 0$  for any finite  $\Lambda$ , is inconsistent with CDF (even when we include 5% systematics in our analysis). Secondly, contours corresponding to 0% and 1% systematics are contained within the 5% systematics band, as expected. In particular, we find that one needs to use  $0.12 \text{ TeV} < \Lambda_{\text{eff}} < 0.35 \text{ TeV}$  (68% CL using 5% systematics) in order to predict the right shift of  $M_W$  at CDF. Of this,  $0.15 \text{ TeV} < \Lambda_{\text{eff}} < 0.35 \text{ TeV}$  is simultaneously allowed by the D0 and CDF measurements.



As opposed to Tevatron, for ATLAS@7 TeV and LHCb we expect the systematics to be much more in control, for reasons already mentioned. Hence, for these, we show results with 0% and 1% systematics only. For both these experiments, we find that there is a wide range of  $\Lambda_{\text{eff}}$  for which the NP hypothesis is allowed by the corresponding measurements of  $M_W$ , namely,  $\Lambda_{\text{eff}} > 0.16$  TeV for ATLAS and  $\Lambda_{\text{eff}} > 0.17$  TeV for LHCb. As expected, the bands are consistent with  $\Delta = 0$  for  $\Lambda_{\text{eff}} \rightarrow \infty$ .

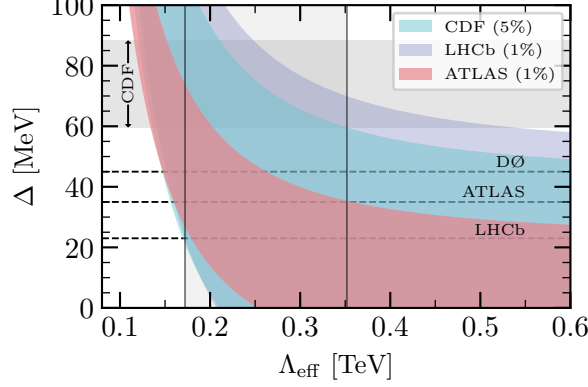


**Figure 3.** 68% bands from all experiments providing  $M_W$  measurement. We show results for 5% systematics for Tevatron (teal) and 1% for both ATLAS (red) and LHCb (violet), overlaid with the experimental measurements ( $1\sigma$ ). The solid vertical lines (grey) give the range of  $\Lambda_{\text{eff}}$  that is simultaneously consistent with all the experiments.

In Figure 3, we simultaneously plot the results obtained from the simulations corresponding to CDF, ATLAS@7 TeV, and LHCb. The shaded bands, teal for CDF, red for ATLAS@7 TeV, and violet for LHCb, show the 68% CL bands obtained by minimizing Equation (6) with respect to the parameter  $\Lambda_{\text{eff}}$ . For CDF, we use 5% systematics per bin, while for ATLAS and LHCb we use 1% systematics. The different bands, overlaid on the measurements, clearly convey the message that there is an overlap between the observations at CDF, ATLAS, and LHCb. This region of overlap (solid vertical gray lines in Figure 3) determines the range for which the NP scenario is ‘consistent’ with all the  $M_W$  measurements (at  $1\sigma$ ) and is given by:

$$0.17 \text{ TeV} < \Lambda_{\text{eff}} < 0.35 \text{ TeV} . \quad (7)$$

Additionally, even if we ignore all systematics for all the experiments and work with only statistical errors, we find that there is a non-zero range which satisfies all experimental measurements, namely  $0.2 \text{ TeV} < \Lambda_{\text{eff}} < 0.22 \text{ TeV}$  at 90% CL.

Before proceeding to the next part of our analysis, note that we have not discussed the measurements by the LEP collaborations [22–25] at all. Given that our NP particle couples only to the quarks, in our hypothesis, we expect the LEP results to remain consistent with the EW precision measurements.

With  $\Lambda_{\text{eff}}$  as determined in Equation (7), we now focus on constraints imposed by experiments performed at similar energy scales as the ones that enter the  $M_W$  measurements, i.e., from high-energy colliders. Two obvious measurements that should constrain the operator in Equation (4) are the following:

- $pp \rightarrow W \rightarrow \ell + p_T^{\text{miss}}$  differential cross-section,
- $pp \rightarrow WW \rightarrow e\mu + p_T^{\text{miss}}$  differential cross section.

Both these measurements have been performed by the ATLAS collaboration using 13 TeV LHC data, the former with  $81 \text{ pb}^{-1}$  of data [69] and the latter with  $36.1 \text{ fb}^{-1}$  of data [70].

We begin the discussion with the single  $W$  channel. Even though the underlying processes corresponding to the  $W$  cross-section measurement and the  $W$  mass measurement are identical, the two analyses are different. For the mass measurement, ATLAS uses the data in the bins given by the fitting ranges (given in Table 1), while the cross-section measurement includes the high momenta data as well. In fact, it is the events in these high momentum bins ( $\gg M_W$ ) that we use to derive the bounds from the  $W$  cross-section data.

Variables	$N_\ell$	$N_J$	$p_T^\ell$	$p_T^{\text{miss}}$	$M_T$	$ \eta^\ell $
Cuts	1	0	$> 25 \text{ GeV}$	$> 25 \text{ GeV}$	$> 50 \text{ GeV}$	$< 2.47$

**Table 2.** Event selection criteria for  $W$  and  $W\Phi$  production at  $\sqrt{s} = 13 \text{ TeV}$ .

To obtain constraints on  $\Lambda_{\text{eff}}$  from this channel, we compare our SM single  $W$  + SM background + NP hypothesis against the experimental observation. For background (SM  $W$  + SM background), we use the data provided in the experiment paper [69] and we simulate the NP contribution  $pp \rightarrow W\Phi + \text{jets}$  in **MadGraph**, followed by **Pythia** for showering and **Delphes** for detector simulations. We use the anti- $k_t$  algorithm [71] with  $p_T^{\text{min}} = 20 \text{ GeV}$ ,  $R = 0.6$  to cluster calorimeter elements within  $|\eta| < 5$ . For subsequent analysis, we impose the same cuts on the kinematic variables ( $\mathcal{X}$ ) and the selection criteria on the number of final state particles as used by ATLAS. These cuts and selection criteria are given in Table 2. Note, in our analysis, we use only the electron channel.

In our study, we use the differential distributions for  $M_T$ ,  $p_T^\ell$ , and  $p_T^{\text{miss}}$  variables. Furthermore, we use the same binning for the variables as the experimental report [69]. Lower bins for all these observables are background-dominated, therefore, we concentrate on the high energy tails and impose analysis level cuts on the variables as follows:

$$M_T > 100 \text{ GeV}; \quad p_T^\ell > 65 \text{ GeV}; \quad p_T^{\text{miss}} > 65 \text{ GeV}. \quad (8)$$

We take the sum of the events in all the bins, passing these cuts, from Reference [69] to constrain our NP scenario and use the Bayesian method to obtain 95% CL exclusions. For the three distinct variables ( $M_T, p_T^\ell, p_T^{\text{miss}}$ ), we get three different limits, given by:

$$\Lambda_{\text{eff}} > \begin{cases} 0.09 \text{ TeV} & : \text{ from } M_T, \\ 0.15 \text{ TeV} & : \text{ from } p_T^\ell, \\ 0.08 \text{ TeV} & : \text{ from } p_T^{\text{miss}}. \end{cases} \quad (9)$$

Clearly,  $p_T^\ell$  provides the most stringent constraint. Unlike  $M_T$  and  $p_T^{\text{miss}}$ , no information about missing transverse momentum is needed to construct  $p_T^\ell$ , leading to less systematics for this variable.

We now move on to the constraints from the  $WW$  cross-section measurement. Similar to the single  $W$  case, we use the background estimates given in the experimental paper [70]. For consistency, we mimic the experimental analysis as far as possible, focusing on the  $pp \rightarrow WW \rightarrow e\mu + p_T^{\text{miss}}$  channel. The collaboration selects events with exactly one hard electron and one hard muon and uses the following variables to characterize these events:

$$\begin{aligned}
p_T^{\text{lead},\ell} &: \text{momentum of the hardest lepton in the event,} \\
p_T^{e\mu} &: \text{transverse momentum of the } e\mu \text{ system,} \\
m_{e\mu} &: \text{invariant mass of the } e\mu \text{ system,} \\
p_{T,\text{track}}^{\text{miss}} &: \text{transverse momentum computed using jet and lepton tracks.}
\end{aligned} \tag{10}$$

In addition, the collaboration imposes a veto on  $b$ -tagged jets with  $p_T > 20$  GeV and  $|\eta| < 2.5$ . For unflavored jets, the veto is for  $p_T > 35$  GeV and  $|\eta| < 4.5$ . In Table 3, we list the kinematic cuts and the selection criteria that the collaboration imposes on the events.

Variables	$N_e$	$N_\mu$	$N_J, N_{J_b}$	$p_T^\ell$	$ \eta^\ell $	$p_{T,\text{miss}}^{\text{track}}$	$p_T^{e\mu}$	$m_{e\mu}$
Cuts	1	1	0	$> 27$ GeV	$< 2.5$	$> 20$ GeV	$> 30$ GeV	$> 55$ GeV

**Table 3.** Event selection criteria for  $WW$  and  $WW\Phi$  production at  $\sqrt{s} = 13$  TeV.

We also impose the same cuts and selection criteria on signal events. For the signal, we simulate  $pp \rightarrow WW\Phi$  in **MadGraph** and allow the  $WW$  system to decay to  $e\mu + p_T^{\text{miss}}$  only. We then pass the simulated parton level events through **Pythia** for subsequent showering and hadronization. Post hadronization and showering, the events are passed through **Delphes**, with the default ATLAS card. Note, in particular, we use the same jet definition as in the single  $W$  analysis.

In computing the  $pp \rightarrow WW\Phi$  cross-section, we find that the amplitude shows a power-law growth with the partonic center-of-mass energy,  $\sqrt{\hat{s}}$ , up to energies much higher than the suppression scale  $\Lambda$  of the irrelevant operator in Equation (4). This growth, beyond the UV cut-off of the theory, is clearly due to the amplitude picking up unphysical modes. This implies that we are extending the amplitude to energies beyond the range of computability of the effective theory. In order to regulate our result and force it to be in the regime of trustable computability, we impose a cut-off on the energy of the NP events following the prescription in Reference [72]. To be specific, we only include NP events for which the invariant mass of the  $WW\Phi$  system (namely,  $M_{WW\Phi}$ ) is less than  $\Lambda$ .

With the cut on  $M_{WW\Phi}$  and the kinematic/selection cuts listed in Table 3 applied to the signal events, we use the differential distribution with respect to  $p_T^{\text{lead},\ell}$  to obtain constraints. We focus on  $p_T^{\text{lead},\ell}$  as the other available distributions (e.g.,  $p_T^{e\mu}$ ,  $m_{e\mu}$ , and angular variables) are less sensitive. Furthermore, ATLAS has much better control over both statistical and systematic uncertainties for the  $p_T^{\text{lead},\ell}$  distributions, compared to the other variables. As mentioned earlier, the NP effects are most prominent in the tails of the momenta distributions. The experimental analysis consolidates the events with  $p_T^{\text{lead},\ell} > 190$  GeV into one ‘overflow’ bin. We use the events in this overflow bin to obtain the exclusion. We use 10% systematics, as reported in Reference [70] for  $p_T^{\text{lead},\ell}$ .

Since we explicitly introduce a scale  $\Lambda$  in our analysis, our result from the di-boson process is qualitatively different from all the earlier results. Earlier, physics was insensitive to the simultaneous scaling of  $\kappa \rightarrow a\kappa$  and  $\Lambda \rightarrow a\Lambda$ , since ultimately  $\Lambda_{\text{eff}} = |\kappa|/\Lambda$  remained invariant. However, the ‘elevation’ of  $\Lambda$  to the role of the explicit cut-off introduces scale dependence. Hence, the constraint obtained from the  $WW$  analysis is *essentially* on the coefficient  $|\kappa|$  for a varying  $\Lambda$ .

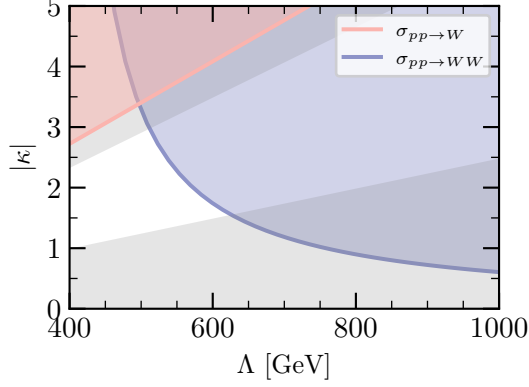


**Figure 4.** Allowed (white) region consistent with all the measurements of  $M_W$  (at  $1\sigma$ ) along with the 95% CL exclusions obtained from ATLAS measurements of  $W \rightarrow \ell + p_T^{\text{miss}}$  (red) and  $WW \rightarrow e\mu + p_T^{\text{miss}}$  (violet) cross sections.

In Figure 4, we show the 95% CL exclusion for 10% systematics, as obtained from this analysis, in the  $|\kappa|$ – $\Lambda$  plane (violet shaded region). The contour tells us what is the maximum  $|\kappa|$  for a given  $\Lambda$ . For example, for  $\Lambda = 1$  TeV, it imposes  $|\kappa| \leq 0.62$ . It is clear from the plot that for the scale below 500 GeV, however, the constraints from  $W$  cross-section measurement become important. Note that, previously we found single  $W$  gives  $\Lambda_{\text{eff}} > 0.15$  TeV from  $p_T^\ell$  measurement. Here, we translate this bound to the  $|\kappa|$ – $\Lambda$  plane (shown in red). In the Figure, we also indicate the region (in gray) ‘disallowed’ from fitting different  $M_W$  measurements taking 5% systematics for CDF and 1% for both ATLAS and LHCb. Given all the exclusions, the region of parameter space allowed (in white) lies between  $1 \lesssim |\kappa| \lesssim 3$  and  $\Lambda \lesssim 0.65$  TeV. Note that, we have checked other exclusive channels with dibosons and jets in the final state [73–76] and find that the bounds discussed here are the strongest.

It is to be noted, the bounds we derive from  $pp$  collisions are different from collider bounds which exist in the literature. The existing bounds do not affect us as these are sensitive to the decay channels of  $\Phi$ , e.g., multi-lepton [77, 78],  $2\ell 2\gamma$  [78], multi-photon [79], and  $2\ell 2h$  [80]. Also,  $\Phi$  couples to the Higgs, the electron, the photon, and gluons only at the order of multi-loops. Therefore, Higgs  $\rightarrow$  invisible bounds [78], constraints from electron colliders and beam dumps (e.g., [81, 82]), and constraints where  $\Phi$  is produced from  $gg$  fusion [83] are not relevant for our NP scenario. Similarly, the  $W$  and  $Z$  boson decay widths are affected either at higher order or with phase space suppressions. Hence, we do not consider these bounds.

After obtaining the allowed range of  $\Lambda_{\text{eff}}$ , we use our NP hypothesis to predict the  $M_W$

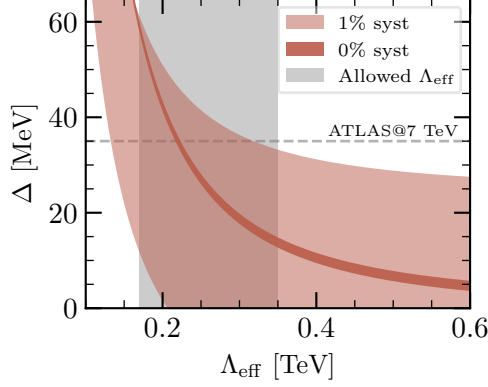


**Figure 5.** Predictions for the expected shift in  $M_W$  ( $\Delta$ ) for ATLAS@13 TeV at  $500 \text{ fb}^{-1}$  (brown band). We also show the range of  $\Lambda_{\text{eff}}$  as allowed from current measurements of  $M_W$  at different colliders. The horizontal dotted line indicates the current measurement of  $\Delta$  at ATLAS@7 TeV.

extraction expected from the 13 TeV LHC data. To be specific, we simulate for the ATLAS detector assuming an integrated luminosity of  $500 \text{ fb}^{-1}$ . Needless to say, although we do not explicitly simulate for CMS, the predictions for ATLAS should act as a proxy for the former as well. We generate the NP events and follow the same prescription as used for the 7 TeV simulations. We use the same cuts, the same fitting ranges, and the same bin widths. From this exercise, we predict (at 68% CL) for LHC@13 TeV the following ranges of  $\Delta$  for two different systematics:

$$\begin{aligned} 13 \text{ MeV} &\lesssim \Delta \lesssim 60 \text{ MeV} & (0\% \text{ systematics}) , \\ 0 \text{ MeV} &\lesssim \Delta \lesssim 61 \text{ MeV} & (1\% \text{ systematics}) . \end{aligned} \quad (11)$$

In Figure 5, we present these contours for 0% (darker brown) and 1% systematics (lighter brown). We also show the range of  $\Lambda_{\text{eff}}$  that is currently allowed (gray band) and the ATLAS@7 TeV measurement ( $1\sigma$ ) of  $M_W$  (dotted lines).

So far in this work, we have outlined an interesting and bare-minimal scenario, which accommodates a remarkable feature that makes the task of extracting  $M_W$  from leptonic decays of  $W$  in hadron colliders highly nontrivial. In fact, conventional strategies with the SM hypothesis simply give an incorrect estimation. The result that the extracted mass depends on the nature of the colliders and/or the center-of-mass energy of collisions is intriguing. The simplicity of the scenario lets it hide from the ensemble of NP searches.

In the remaining part of this work, we speculate about the nature/ultraviolet aspects of the scenario. Even though we do not suggest particular renormalizable UV completions of Equation (4), our discussion here is geared towards finding possible further constructions, still in terms of irrelevant operators, that address questions regarding the EW symmetry and the flavor symmetry. As we show now, there is a multitude of possibilities even at this intermediate level. Finding and classifying all possible renormalizable UV completions is a completely different task and we leave it for future endeavors.

We begin this exercise by noting that in case the complex parameter  $\kappa$  is purely imaginary (*i.e.*,  $\kappa = ik/\sqrt{2}$ ), the theory described in Equation (4) is equivalent to more

familiar constructions of Axion Like Particles (ALPs). A field-dependent redefinition of left-handed  $u$  and  $d$  quarks eliminates the operator in Equation (4) but gives rise to new ones:

$$\begin{aligned} u_L &\rightarrow \exp\left(+\frac{ik\Phi}{f_\Phi}\right) u_L \quad \text{and} \quad d_L \rightarrow \exp\left(-\frac{ik\Phi}{f_\Phi}\right) d_L \quad \text{where} \quad f_\Phi = 2\Lambda \\ \delta\mathcal{L} &= k\frac{\partial_\mu\Phi}{f_\Phi} (\bar{u}_L\gamma^\mu u_L - \bar{d}_L\gamma^\mu d_L) + k\frac{i\Phi}{f_\Phi} \left(1 + \frac{h}{v}\right) (m_u \bar{u}u - m_d \bar{d}d) + \dots, \end{aligned} \quad (12)$$

where  $\dots$  represent additional terms of order  $(\Phi/f_\Phi)^2$  or more, and terms suppressed by at least one power of  $16\pi^2$ . The redefinition we use is chiral in nature, and hence the anomaly associated with the electromagnetic current gives rise to operators  $\Phi F\tilde{F}$ . Note, no  $\Phi G\tilde{G}$  is generated since the redefinition includes opposite (field dependent) phases for  $u_L$  and  $d_L$ . Even the mass-dependent operators and the  $\Phi F\tilde{F}$  term do not seem independent. A suitable redefinition of the right-handed quarks can eliminate the mass-terms in Equation (12) as well as the anomaly term, at the cost of a new term involving  $\partial\Phi$ . Note that, we can reach the same cleaner-looking Lagrangian, if we employ rather a vectorial redefinition of  $u$  and  $d$  quarks (instead of the chiral ones in Equation (12)).

$$\begin{aligned} u &\rightarrow \exp\left(+\frac{ik\Phi}{f_\Phi}\right) u \quad \text{and} \quad d \rightarrow \exp\left(-\frac{ik\Phi}{f_\Phi}\right) d \quad \text{where} \quad f_\Phi = 2\Lambda \\ \delta\mathcal{L} &= k\frac{\partial_\mu\Phi}{f_\Phi} (\bar{u}\gamma^\mu u - \bar{d}\gamma^\mu d). \end{aligned} \quad (13)$$

As mentioned earlier, these recasts bring the unusual operator in Equation (4) in the well-studied paradigm of the ALP physics and make the task of building further models and deriving constraints simpler. The guiding principle for building the UV model which will give rise to the apparent shift of  $W$ -mass is, therefore, straightforward – the UV model must result in Equation (4) *and/or* the derivative operator in Equation (12) in terms of left-handed quarks, but there should not be any quark field redefinitions that can eliminate both at the same time. Consequently, for the rest of this work, we use the derivative operator in Equation (12) as the starting point for further constructions while discussing issues of flavor and EW symmetry. Generalizing it in the flavor space, we write the operator in a convenient manner:

$$\delta\mathcal{L} = \sum_{ij} k_{ij} \frac{\partial_\mu\Phi}{f_\Phi} \bar{q}_{L_i} \gamma^\mu \sigma^3 q_{L_j}, \quad (14)$$

where  $i, j$  are flavor indices,  $q_L$  represent the usual left-handed doublets, and  $\sigma^3$  is the Pauli matrix. It allows us to jump directly into the flavor question. Arbitrary  $k_{ij}$  is simply ruled out from large flavor-changing neutral currents (FCNCs) (for a recent review see Reference [84]). The UV model must include considerations from the flavor sector. A safer ansatz is using  $k_{ij} = k \delta_{ij}$  – which does not give rise to any new flavor-breaking spurions\*. However, given specific models, one might require small non-diagonal  $k_{ij}$  elements to counter loop-induced FCNCs.

---

\*Note that bringing in additional quark flavors changes the best fit and exclusion plots in Figure 2-4, where the biggest effect arises because of the strange quark. Converting in the basis of Equation (4), one finds additional operator with the replacement of  $V_{ud}^{\text{CKM}} d_L \rightarrow V_{us}^{\text{CKM}} s_L$ .

The left-handed quark doublets are also electroweak doublets and the operators in Equation (14) also violate electroweak symmetry. Not surprisingly, the imposition that Equation (14) arises from a fully electroweak theory is a lot more demanding. The simplest construct is to take  $k/f_\Phi$  to be proportional to the Higgs vacuum expectation value (vev)  $v$ . For example, when the Higgs is replaced with its vev, the following electroweak operator yields Equation (14):

$$\bar{k} \frac{1}{\bar{\Lambda}^3} \partial_\mu \Phi \sum_a H^\dagger \sigma^a H \bar{q}_L \gamma^\mu \sigma^a q_L \Rightarrow \frac{k}{f_\Phi} = \bar{k} \frac{1}{\bar{\Lambda}} \left( \frac{v/\sqrt{2}}{\bar{\Lambda}} \right)^2. \quad (15)$$

This scheme finds the dimension  $D = 5$  operator from a truly  $D = 7$  operator. Because of this, one expects the scale in the UV (namely,  $\bar{\Lambda}$ ) to be far more suppressed than the apparent scale  $f_\Phi$  as long as one takes  $k \sim \bar{k}$ . This seemingly low  $\bar{\Lambda}$  may not necessarily mean the existence of additional new degrees of freedom at low energies. For explicit construct, see, for example, Reference [85] which, in fact, deals with ALP-like scenarios.

A far more creative and attractive avenue is to have the coupling in Equation (14) from an electroweak  $D = 5$  operator. This requires an electroweak triplet  $\Sigma \equiv \Sigma_a t^a \equiv \{\Sigma_\pm, \Sigma_3\}$ .

$$\delta\mathcal{L} = \bar{k} \frac{1}{\bar{\Lambda}} \sum_a \partial_\mu \Sigma_a \bar{q}_L \gamma^\mu \sigma^a q_L. \quad (16)$$

Further model building is necessary to accommodate  $\Sigma_\pm$ , since these have to be heavier than the EW scale to avoid bounds from  $W/Z$  widths. The light neutral state ( $\Phi$ ) can be obtained by introducing another electroweak singlet (say  $\Sigma_0$ ). It is trivial to design a potential (using only marginal and relevant operators) with the  $\Sigma$  fields and the Higgs field, where one obtains a near massless light scalar after the Higgs is replaced by its vev. This requires choosing coupling constants for different operators suitably and also cancelling quantum corrections with bare terms. Since we give no importance to the amount of ‘naturalness’ we do not foresee any problem with constructing a model in these lines.

The lack of a concrete model makes a discussion about contributions to the EW T-parameter moot. Any positive contribution to the T parameter from the triplet [86, 87] can be counteracted by the presence of heavy fermions or kinetic mixing (see, e.g., [88–91]), which might be present in the UV model. Also, one can not but notice that the phenomenological constraints and best fit values for  $W$ -mass measurements will be much different for any of these UV scenarios here. For example, one has to take into account  $\Sigma_\pm$  contributions to  $p + \bar{p}(p) \rightarrow \Phi + W$  to re-derive the best fit plots, find constraints on the mass of  $\Sigma_\pm$ , and look for additional signals via which the model might present chances for it being discovered at the LHC. All these discussions are beyond the scope of this work. Similarly, a proper discussion of flavor constraints (see, e.g., [84, 92–94]), should include a full model—that determines relationships between the different parameters and also the running of the couplings to low energies.

In conclusion, the peculiarity of the CDF measurement of  $M_W$  lies not only in the fact that it deviates in a statistically significant way from the electroweak precision fits but also in the fact that it drifts away from measurements reported by other experimental



collaborations. We have proposed a simple extension of the Standard Model where the addition of a singular source of unaccounted-for missing transverse momentum can give rise to the discrepant extractions of  $M_W$  across the different experiments. We emphasize that the model presented here is a “proof-of-principle” which quantitatively and qualitatively demonstrates the effects of misinterpreting the observed missing momentum on the determination of the seemingly pure SM observable (such as  $M_W$ ). Of course, other classes of models may exist which, by leading to similar misinterpretations, could explain this discrepancy. The prediction that the  $M_W$  obtained through template fits depends on the nature of colliders is spectacular and has far-reaching consequences. It implies that before all these models are ruled out, one cannot simply take the disagreement between two experiments to indicate that one of the experiments must be wrong—in this regard, the  $M_W$  discrepancy might be a hint of a much broader and enriching theme.

## Acknowledgments

We would like to thank Rick S. Gupta for helpful discussions, Gautam Bhattacharyya and Debajyoti Choudhury for comments on an earlier version of the draft. We acknowledge the computational facility provided by the Department of Theoretical Physics at TIFR. Part of this work was completed and benefitted from discussions held at the workshop “Particle Physics: Phenomena, Puzzles, Promises” (Code:ICTS/p2p3/11) hosted by ICTS, TIFR.

## Appendix: Additional considerations for the CDF analyses

In this Appendix, we discuss some subtleties related to our CDF analyses. We have discussed the methodology in the text itself and argued in favor of the validity of our analysis. However, as we are unable to incorporate some aspects of detector simulations and statistical nuances, we perform additional checks to establish the robustness of our results.

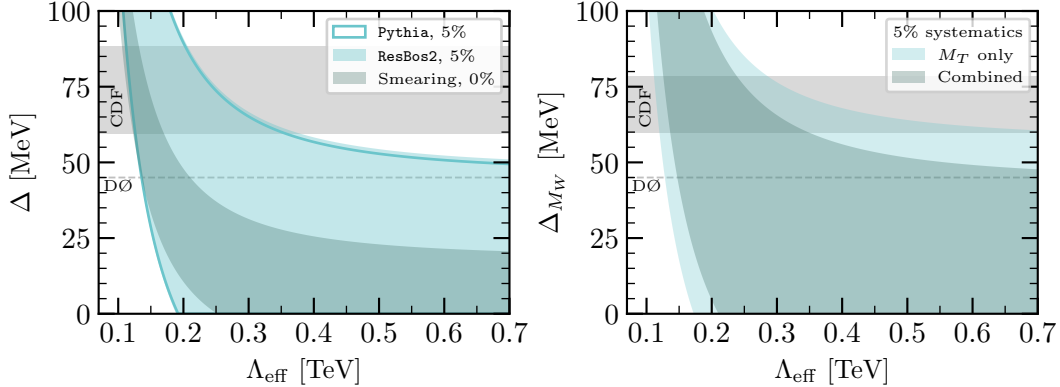


**Figure 6.** *Left:* 68% bands using *Pythia* results only (with 5% systematics) (transparent, solid boundaries), using *Pythia* + *ResBos2* (5% systematics) (lighter shade), and *Pythia* + *ResBos2* + smearing (0% systematics) (darker shade). For all three bands, we use the  $M_T$  distributions only. *Right:* 68% CL bands obtained by using the  $M_T$  variable only (lighter shade) and the one with all kinematic variables ( $M_T, p_T^\ell, p_T^{\text{miss}}$ ) combined.

To verify that the systematics used by us captures the effects of detector smearing and final state radiations, we perform an auxiliary analysis. In this analysis, we find the 68% CL bands on  $\Lambda_{\text{eff}}$  after the convolution of the `Pythia` output with both the smeared and unsmeared `ResBos2` factors [68]. As smearing affects  $M_T$  the most [68], we use only  $M_T$  for this study. In the left panel of Figure 6, we plot these bands with 5% systematics for the unsmeared case (lighter shade) and without systematics for the smeared case (darker shade). For reference, we also show the band obtained using only the `Pythia` output (solid borders). From the Figure, it is clear that the effect of smearing is encapsulated by the band with no smearing but with 5% systematics.

As a second check, we compare the 68% CL bands on  $\Lambda_{\text{eff}}$  obtained using only  $M_T$  and the band obtained by combining all the kinematic variables  $\{M_T, p_T^\ell, p_T^{\text{miss}}\}$ . In the right panel of Figure 6, we show these bands for the best fit obtained by using only  $M_T$  (lighter shade) and all the variables (darker shade). As expected, we get a tighter band for the case where all the variables are combined. These comparisons ensure that the correlations between the different variables, which we cannot take into account, do not substantially modify our conclusions.

## References

- [1] PARTICLE DATA GROUP collaboration, *Review of Particle Physics*, [PTEP \*\*2022\*\* \(2022\) 083C01](#).
- [2] T. Bose et al., *Report of the Topical Group on Physics Beyond the Standard Model at Energy Frontier for Snowmass 2021*, [2209.13128](#).
- [3] P.J. Fox et al., *TF08 Snowmass Report: BSM Model Building*, [2210.03075](#).
- [4] ATLAS collaboration, *SUSY Summary Plots March 2022*, Tech. Rep. [ATL-PHYS-PUB-2022-013](#), CERN, Geneva (2022).
- [5] ATLAS collaboration, *Summary plots for beyond Standard Model Higgs boson benchmarks for direct and indirect searches*, Tech. Rep. [ATL-PHYS-PUB-2022-043](#), CERN, Geneva (2022).
- [6] ATLAS collaboration, *Dark matter summary plots for s-channel mediators*, Tech. Rep. [ATL-PHYS-PUB-2020-021](#), CERN, Geneva (2020).
- [7] ATLAS collaboration, *Summary Plots for Heavy Particle Searches and Long-lived Particle Searches - March 2022*, Tech. Rep. [ATL-PHYS-PUB-2022-011](#), CERN, Geneva (2022).
- [8] ATLAS collaboration, *Summary of Diboson Resonance Searches from the ATLAS Experiment*, Tech. Rep. [ATL-PHYS-PUB-2021-018](#), CERN, Geneva (2021).
- [9] CMS collaboration, *Searches for Extended Higgs Sectors at CMS*, [PoS ICHEP2022 \(2022\) 511](#).
- [10] ATLAS, CMS, LHCb collaboration, *Highlights on Supersymmetry and Exotic Searches at the LHC*, in *32nd Rencontres de Blois on Particle Physics and Cosmology*, 4, 2022 [[2204.03053](#)].
- [11] CMS collaboration, *Constraining challenging regions of the SUSY parameter space with the CMS experiment*, [PoS EPS-HEP2021 \(2022\) 659](#).

- [12] ATLAS, CMS, LHCb collaboration, *Searches for Exotica*, *PoS EPS-HEP2021* (2022) 035.
- [13] CMS collaboration, *Search for  $W'$  bosons decaying to a top and a bottom quark at  $\sqrt{s}=13$  TeV in the hadronic final state with CMS*, *PoS LHCP2021* (2021) 207.
- [14] ATLAS, CMS, LHCb collaboration, *Flavour anomalies: a review*, *J. Phys. Conf. Ser.* **1137** (2019) 012025 [[1807.11373](#)].
- [15] D. London and J. Matias, *B Flavour Anomalies: 2021 Theoretical Status Report*, *Ann. Rev. Nucl. Part. Sci.* **72** (2022) 37 [[2110.13270](#)].
- [16] MUON G-2 collaboration, *Measurement of the Positive Muon Anomalous Magnetic Moment to 0.46 ppm*, *Phys. Rev. Lett.* **126** (2021) 141801 [[2104.03281](#)].
- [17] A.G. Riess et al., *New Parallaxes of Galactic Cepheids from Spatially Scanning the Hubble Space Telescope: Implications for the Hubble Constant*, *Astrophys. J.* **855** (2018) 136 [[1801.01120](#)].
- [18] CDF collaboration, *High-precision measurement of the  $W$  boson mass with the CDF II detector*, *Science* **376** (2022) 170.
- [19] ATLAS collaboration, *Measurement of the  $W$ -boson mass in  $pp$  collisions at  $\sqrt{s} = 7$  TeV with the ATLAS detector*, *Eur. Phys. J. C* **78** (2018) 110 [[1701.07240](#)].
- [20] LHCb collaboration, *Measurement of the  $W$  boson mass*, *JHEP* **01** (2022) 036 [[2109.01113](#)].
- [21] J. de Blas, M. Ciuchini, E. Franco, A. Goncalves, S. Mishima, M. Pierini et al., *Global analysis of electroweak data in the Standard Model*, *Phys. Rev. D* **106** (2022) 033003 [[2112.07274](#)].
- [22] OPAL collaboration, *Measurement of the mass and width of the  $W$  boson*, *Eur. Phys. J. C* **45** (2006) 307 [[hep-ex/0508060](#)].
- [23] L3 collaboration, *Measurement of the mass and the width of the  $W$  boson at LEP*, *Eur. Phys. J. C* **45** (2006) 569 [[hep-ex/0511049](#)].
- [24] ALEPH collaboration, *Measurement of the  $W$  boson mass and width in  $e^+e^-$  collisions at LEP*, *Eur. Phys. J. C* **47** (2006) 309 [[hep-ex/0605011](#)].
- [25] DELPHI collaboration, *Measurement of the Mass and Width of the  $W$  Boson in  $e^+e^-$  Collisions at  $\sqrt{s} = 161\text{-GeV} - 209\text{-GeV}$* , *Eur. Phys. J. C* **55** (2008) 1 [[0803.2534](#)].
- [26] P. Asadi, C. Cesarotti, K. Fraser, S. Homiller and A. Parikh, *Oblique Lessons from the  $W$  Mass Measurement at CDF II*, [2204.05283](#).
- [27] L.M. Carpenter, T. Murphy and M.J. Smylie, *Changing patterns in electroweak precision fits with new color-charged states: Oblique corrections and the  $W$ -boson mass*, *Phys. Rev. D* **106** (2022) 055005 [[2204.08546](#)].
- [28] Y.-Z. Fan, T.-P. Tang, Y.-L.S. Tsai and L. Wu, *Inert Higgs Dark Matter for CDF II  $W$ -Boson Mass and Detection Prospects*, *Phys. Rev. Lett.* **129** (2022) 091802 [[2204.03693](#)].
- [29] C.-R. Zhu, M.-Y. Cui, Z.-Q. Xia, Z.-H. Yu, X. Huang, Q. Yuan et al.,  *$\text{GeV}$  antiproton/gamma-ray excesses and the  $W$ -boson mass anomaly: three faces of  $\sim 60 - 70$  GeV dark matter particle?*, [2204.03767](#).
- [30] B.-Y. Zhu, S. Li, J.-G. Cheng, R.-L. Li and Y.-F. Liang, *Using gamma-ray observation of dwarf spheroidal galaxy to test a dark matter model that can interpret the  $W$ -boson mass anomaly*, [2204.04688](#).

- [31] J. Kawamura, S. Okawa and Y. Omura, *W boson mass and muon  $g-2$  in a lepton portal dark matter model*, *Phys. Rev. D* **106** (2022) 015005 [2204.07022].
- [32] P. Mondal, *Enhancement of the W boson mass in the Georgi-Machacek model*, *Phys. Lett. B* **833** (2022) 137357 [2204.07844].
- [33] K.I. Nagao, T. Nomura and H. Okada, *A model explaining the new CDF II W boson mass linking to muon  $g-2$  and dark matter*, 2204.07411.
- [34] K.-Y. Zhang and W.-Z. Feng, *Explaining W boson mass anomaly and dark matter with a  $U(1)$  dark sector*, 2204.08067.
- [35] X. Liu, S.-Y. Guo, B. Zhu and Y. Li, *Correlating Gravitational Waves with W-boson Mass, FIMP Dark Matter, and Majorana Seesaw Mechanism*, *Sci. Bull.* **67** (2022) 1437 [2204.04834].
- [36] K. Sakurai, F. Takahashi and W. Yin, *Singlet extensions and W boson mass in light of the CDF II result*, *Phys. Lett. B* **833** (2022) 137324 [2204.04770].
- [37] H. Song, W. Su and M. Zhang, *Electroweak phase transition in 2HDM under Higgs, Z-pole, and W precision measurements*, *JHEP* **10** (2022) 048 [2204.05085].
- [38] H. Bahl, J. Braathen and G. Weiglein, *New physics effects on the W-boson mass from a doublet extension of the SM Higgs sector*, *Phys. Lett. B* **833** (2022) 137295 [2204.05269].
- [39] Y. Cheng, X.-G. He, Z.-L. Huang and M.-W. Li, *Type-II seesaw triplet scalar effects on neutrino trident scattering*, *Phys. Lett. B* **831** (2022) 137218 [2204.05031].
- [40] K.S. Babu, S. Jana and V.P. K., *Correlating W-Boson Mass Shift with Muon  $g-2$  in the Two Higgs Doublet Model*, *Phys. Rev. Lett.* **129** (2022) 121803 [2204.05303].
- [41] Y. Heo, D.-W. Jung and J.S. Lee, *Impact of the CDF W-mass anomaly on two Higgs doublet model*, *Phys. Lett. B* **833** (2022) 137274 [2204.05728].
- [42] Y.H. Ahn, S.K. Kang and R. Ramos, *Implications of the new CDF II W-boson mass on two-Higgs-doublet models*, *Phys. Rev. D* **106** (2022) 055038 [2204.06485].
- [43] M.-D. Zheng, F.-Z. Chen and H.-H. Zhang, *The  $W\ell\nu$ -vertex corrections to W-boson mass in the R-parity violating MSSM*, 2204.06541.
- [44] P. Fileviez Perez, H.H. Patel and A.D. Plascencia, *On the W mass and new Higgs bosons*, *Phys. Lett. B* **833** (2022) 137371 [2204.07144].
- [45] S. Kanemura and K. Yagyu, *Implication of the W boson mass anomaly at CDF II in the Higgs triplet model with a mass difference*, *Phys. Lett. B* **831** (2022) 137217 [2204.07511].
- [46] G. Arcadi and A. Djouadi, *The 2HD+a model for a combined explanation of the possible excesses in the CDF  $M_W$  measurement and  $(g-2)_\mu$  with Dark Matter*, 2204.08406.
- [47] X.-F. Han, F. Wang, L. Wang, J.M. Yang and Y. Zhang, *Joint explanation of W-mass and muon  $g-2$  in the 2HDM\**, *Chin. Phys. C* **46** (2022) 103105 [2204.06505].
- [48] J.-W. Wang, X.-J. Bi, P.-F. Yin and Z.-H. Yu, *Electroweak dark matter model accounting for the CDF W-mass anomaly*, *Phys. Rev. D* **106** (2022) 055001 [2205.00783].
- [49] H. Bahl, W.H. Chiu, C. Gao, L.-T. Wang and Y.-M. Zhong, *Tripling down on the W boson mass*, *Eur. Phys. J. C* **82** (2022) 944 [2207.04059].
- [50] J. Butterworth, J. Heeck, S.H. Jeon, O. Mattelaer and R. Ruiz, *Testing the Scalar Triplet Solution to CDF's Fat W Problem at the LHC*, 2210.13496.

- [51] C.-T. Lu, L. Wu, Y. Wu and B. Zhu, *Electroweak precision fit and new physics in light of the  $W$  boson mass*, *Phys. Rev. D* **106** (2022) 035034 [[2204.03796](#)].
- [52] J. de Blas, M. Pierini, L. Reina and L. Silvestrini, *Impact of the recent measurements of the top-quark and  $W$ -boson masses on electroweak precision fits*, [2204.04204](#).
- [53] A. Strumia, *Interpreting electroweak precision data including the  $W$ -mass CDF anomaly*, *JHEP* **08** (2022) 248 [[2204.04191](#)].
- [54] E. Bagnaschi, J. Ellis, M. Madigan, K. Mimasu, V. Sanz and T. You, *SMEFT analysis of  $m_W$* , *JHEP* **08** (2022) 308 [[2204.05260](#)].
- [55] J. Fan, L. Li, T. Liu and K.-F. Lyu,  *$W$ -Boson Mass, Electroweak Precision Tests and SMEFT*, [2204.04805](#).
- [56] J. Gu, Z. Liu, T. Ma and J. Shu, *Speculations on the  $W$ -Mass Measurement at CDF*, [2204.05296](#).
- [57] R. Balkin, E. Madge, T. Menzo, G. Perez, Y. Soreq and J. Zupan, *On the implications of positive  $W$  mass shift*, *JHEP* **05** (2022) 133 [[2204.05992](#)].
- [58] R.S. Gupta, *Running away from the  $T$ -parameter solution to the  $W$  mass anomaly*, [2204.13690](#).
- [59] J. Gao, D. Liu and K. Xie, *Understanding PDF uncertainty on the  $W$  boson mass measurements in CT18 global analysis*, [2205.03942](#).
- [60] E.d.S. Almeida, A. Alves, O.J.P. Eboli and M.C. Gonzalez-Garcia, *Impact of CDF-II measurement of  $M_W$  on the electroweak legacy of the LHC Run II*, [2204.10130](#).
- [61] J. Alwall, M. Herquet, F. Maltoni, O. Mattelaer and T. Stelzer, *MadGraph 5 : Going Beyond*, *JHEP* **06** (2011) 128 [[1106.0522](#)].
- [62] R.D. Ball et al., *Parton distributions with LHC data*, *Nucl. Phys. B* **867** (2013) 244 [[1207.1303](#)].
- [63] NNPDF collaboration, *Parton distributions for the LHC Run II*, *JHEP* **04** (2015) 040 [[1410.8849](#)].
- [64] C. Bierlich et al., *A comprehensive guide to the physics and usage of PYTHIA 8.3*, [2203.11601](#).
- [65] M.L. Mangano, M. Moretti, F. Piccinini and M. Treccani, *Matching matrix elements and shower evolution for top-quark production in hadronic collisions*, *JHEP* **01** (2007) 013 [[hep-ph/0611129](#)].
- [66] DELPHES 3 collaboration, *DELPHES 3, A modular framework for fast simulation of a generic collider experiment*, *JHEP* **02** (2014) 057 [[1307.6346](#)].
- [67] J.P. Isaacson, *ResBos2: Precision Resummation for the LHC ERA*, Ph.D. thesis, Michigan State University, Jan., 2017.
- [68] J. Isaacson, Y. Fu and C.P. Yuan, *ResBos2 and the CDF  $W$  Mass Measurement*, [2205.02788](#).
- [69] ATLAS collaboration, *Measurement of  $W^\pm$  and  $Z$ -boson production cross sections in  $pp$  collisions at  $\sqrt{s} = 13$  TeV with the ATLAS detector*, *Phys. Lett. B* **759** (2016) 601 [[1603.09222](#)].
- [70] ATLAS collaboration, *Measurement of fiducial and differential  $W^+W^-$  production*

- cross-sections at  $\sqrt{s} = 13$  TeV with the ATLAS detector, *Eur. Phys. J. C* **79** (2019) 884 [[1905.04242](#)].
- [71] M. Cacciari, G.P. Salam and G. Soyez, *The anti- $k_t$  jet clustering algorithm*, *JHEP* **04** (2008) 063 [[0802.1189](#)].
  - [72] R. Franceschini, G. Panico, A. Pomarol, F. Riva and A. Wulzer, *Electroweak Precision Tests in High-Energy Diboson Processes*, *JHEP* **02** (2018) 111 [[1712.01310](#)].
  - [73] ATLAS collaboration, *Search for the electroweak diboson production in association with a high-mass dijet system in semileptonic final states in pp collisions at  $\sqrt{s} = 13$  TeV with the ATLAS detector*, *Phys. Rev. D* **100** (2019) 032007 [[1905.07714](#)].
  - [74] ATLAS collaboration, *Observation of electroweak production of a same-sign W boson pair in association with two jets in pp collisions at  $\sqrt{s} = 13$  TeV with the ATLAS detector*, *Phys. Rev. Lett.* **123** (2019) 161801 [[1906.03203](#)].
  - [75] CMS collaboration, *First observation of the electroweak production of a leptonically decaying  $W^+ W^-$  pair in association with two jets in  $\sqrt{s} = 13$  TeV pp collisions.*, .
  - [76] CMS collaboration, *Measurements of production cross sections of WZ and same-sign WW boson pairs in association with two jets in proton-proton collisions at  $\sqrt{s} = 13$  TeV*, *Phys. Lett. B* **809** (2020) 135710 [[2005.01173](#)].
  - [77] CMS collaboration, *Search for a low-mass dilepton resonance in Higgs boson decays to four-lepton final states at  $\sqrt{s} = 13$  TeV*, .
  - [78] M. Bauer, M. Neubert and A. Thamm, *Collider Probes of Axion-Like Particles*, *JHEP* **12** (2017) 044 [[1708.00443](#)].
  - [79] D. d’Enterria, *Collider constraints on axion-like particles*, in *Workshop on Feebly Interacting Particles*, 2, 2021 [[2102.08971](#)].
  - [80] ATLAS collaboration, *Search for Higgs Boson Decays into a Z Boson and a Light Hadronically Decaying Resonance Using 13 TeV pp Collision Data from the ATLAS Detector*, *Phys. Rev. Lett.* **125** (2020) 221802 [[2004.01678](#)].
  - [81] D.S.M. Alves and N. Weiner, *A viable QCD axion in the MeV mass range*, *JHEP* **07** (2018) 092 [[1710.03764](#)].
  - [82] L. Darmé, F. Giacchino, E. Nardi and M. Raggi, *Invisible decays of axion-like particles: constraints and prospects*, *JHEP* **06** (2021) 009 [[2012.07894](#)].
  - [83] S. Carra, V. Goumarre, R. Gupta, S. Heim, B. Heinemann, J. Kuechler et al., *Constraining off-shell production of axionlike particles with  $Z\gamma$  and WW differential cross-section measurements*, *Phys. Rev. D* **104** (2021) 092005 [[2106.10085](#)].
  - [84] M. Bauer, M. Neubert, S. Renner, M. Schnubel and A. Thamm, *Flavor probes of axion-like particles*, *JHEP* **09** (2022) 056 [[2110.10698](#)].
  - [85] A. Hook, *Naturalness without new particles*, *JHEP* **04** (2021) 048 [[1902.06758](#)].
  - [86] J.R. Forshaw, A. Sabio Vera and B.E. White, *Mass bounds in a model with a triplet Higgs*, *JHEP* **06** (2003) 059 [[hep-ph/0302256](#)].
  - [87] M.-C. Chen, S. Dawson and C.B. Jackson, *Higgs Triplets, Decoupling, and Precision Measurements*, *Phys. Rev. D* **78** (2008) 093001 [[0809.4185](#)].
  - [88] E. Gates and J. Terning, *Negative contributions to S from Majorana particles*, *Phys. Rev. Lett.* **67** (1991) 1840.



- [89] P.Q. Hung, R. McCoy and D. Singleton, *Negative delta rho with four families in the Standard Model*, *Phys. Rev. D* **50** (1994) 2082.
- [90] B. Holdom, *Negative  $T$  from a dynamical left-handed neutrino mass*, *Phys. Rev. D* **54** (1996) R721 [[hep-ph/9602248](#)].
- [91] T. Gregoire, D. Tucker-Smith and J.G. Wacker, *What precision electroweak physics says about the  $SU(6)$  /  $Sp(6)$  little Higgs*, *Phys. Rev. D* **69** (2004) 115008 [[hep-ph/0305275](#)].
- [92] W. Altmannshofer, S. Gori and D.J. Robinson, *Constraining axionlike particles from rare pion decays*, *Phys. Rev. D* **101** (2020) 075002 [[1909.00005](#)].
- [93] T. Bandyopadhyay, S. Ghosh and T.S. Roy, *ALP-Pions generalized*, *Phys. Rev. D* **105** (2022) 115039 [[2112.13147](#)].
- [94] W. Altmannshofer, J.A. Dror and S. Gori, *New Insights Into Axion-Lepton Interactions*, [2209.00665](#).